

Higgs production in gluon fusion at next-to-next-to-leading order QCD for finite top mass

Robert V. Harlander⁽¹⁾, Hendrik Mantler⁽¹⁾, Simone Marzani⁽²⁾, Kemal J. Ozeren⁽¹⁾

⁽¹⁾*Fachbereich C, Bergische Universität Wuppertal
42097 Wuppertal, Germany*

⁽²⁾*School of Physics & Astronomy, University of Manchester,
Manchester M13 9PL, United Kingdom*

Abstract

The inclusive Higgs production cross section from gluon fusion is calculated through NNLO QCD, including its top quark mass dependence. This is achieved through a matching of the $1/M_t$ expansion of the partonic cross sections to the exact large- \hat{s} limits which are derived from k_T -factorization. The accuracy of this procedure is estimated to be better than 1% for the hadronic cross section. The final result is shown to be within 1% of the commonly used effective theory approach, thus confirming earlier findings.

1 Introduction

It is well-known that a reliable quantitative prediction of the gluon fusion production cross section for Higgs bosons requires a next-to-next-to-leading order (NNLO) calculation (for a review on Higgs physics, see Refs. [1, 2]). However, since it is a loop-induced process, its NNLO correction requires a three-loop calculation of a $2 \rightarrow 1$ process. Fortunately, it was found at next-to-leading order (NLO) [3, 4, 5] that the perturbative K-factor is very well reproduced in the so-called *effective field theory* (EFT) *approach*, where the gluon-Higgs coupling is taken into account by an effective Lagrangian

$$\mathcal{L}_{\text{eff}} = -\frac{H}{4v} C_1 G_{\mu\nu} G^{\mu\nu}, \quad (1)$$

with H the Higgs field, $G_{\mu\nu}$ the gluonic field strength tensor, $v = 246 \text{ GeV}$ the vacuum expectation value of the Higgs field, and C_1 a perturbatively evaluated Wilson coefficient (see, e.g., Ref. [6, 7]). The NLO cross section in the EFT approach is then obtained by scaling the LO cross section (obtained in the full theory) with the effective NLO K-factor.

Although, to our knowledge, a quantitative understanding of the accuracy of this approach is still missing (in the sense that there is no error estimate), the observed difference of less than 1% to the full NLO cross section (which is known in numerical form [8]) for $M_H < 2M_t$ was considered to be sufficiently convincing in order to trust the EFT approach also at NNLO.

Apart from the inclusive NNLO calculation [9, 10, 11], the heavy-top limit has also been used for distributions, resummations, and even fully differential quantities at NNLO (for a review, see Ref. [12]). It is therefore of the utmost importance to justify the validity of the EFT approach. This has been first achieved at NNLO in Ref. [13, 14, 15, 16] by an expansion of the relevant Feynman diagrams in the limit $M_H^2, \hat{s} \ll M_t^2$, where $\sqrt{\hat{s}}$ is the partonic center-of-mass energy. The apparent failure of this expansion for large \hat{s} (which is only restricted by the hadronic center-of-mass energy squared, s) is only partly cured by the strong suppression of the parton luminosity. The prediction of the gg channel contribution, which accounts for more than 95% of the NLO hadronic cross section, was additionally treated by matching to the known large- \hat{s} behaviour [17]. The other channels, for which the large- \hat{s} behaviour is not known, were treated by including only those terms in the $1/M_t$ expansion up to which the series was observed to converge. It was found that the resulting cross section agrees with the EFT result to better than 1% over the relevant mass range between 100 and 300 GeV.

In this paper, we extend the analysis of Refs. [13, 15, 17] by deriving the high-energy limits of the other channels as well. This leads to a significant stabilization of the qg channel which contributes about 2-5% to the total NLO cross section. The peculiar threshold behaviour of the quark–anti-quark channel prohibits a reasonable approximation from the high- and the low-energy information alone, but its contribution is in any case only at the per-mille level. We can therefore safely claim to present a stable prediction for the total cross section including top quark mass effects for Higgs masses between 100 and 300 GeV.

2 Preliminaries

2.1 Notation

For the convenience of the reader, let us outline the notation at the very beginning. The Higgs mass is denoted by M_H , the on-shell top quark mass by M_t , and the hadronic and the partonic center of mass energies are s and \hat{s} , respectively. Unless indicated otherwise, $\alpha_s \equiv \alpha_s^{(5)}(\mu_R^2)$ denotes the strong coupling in the $\overline{\text{MS}}$ scheme for five active flavours at the renormalization scale μ_R . The following variables will turn out to be useful throughout

the text:

$$\begin{aligned}
z &= \frac{M_H^2}{s}, & x &= \frac{M_H^2}{\hat{s}}, & \tau &= \frac{4M_t^2}{M_H^2}, & \omega &= \frac{\hat{s}}{s}. \\
l_F &= \ln \frac{\mu_F^2}{M_H^2} & l_R &= \ln \frac{\mu_R^2}{M_H^2} & l_t &= \ln \frac{M_t^2}{M_H^2},
\end{aligned} \tag{2}$$

with the factorization scale μ_F .

The inclusive hadronic cross section $\sigma_{pp'}$ for Standard Modell Higgs production in proton–(anti-)proton collisions is obtained by convoluting the partonic cross section $\hat{\sigma}_{\alpha\beta}$ for the scattering of parton α with parton β by the corresponding parton density functions $\phi_{\alpha/p}(x)$ (PDFs):

$$\begin{aligned}
\sigma_{\alpha\beta}(z, \tau, l_F) &= \int_z^1 d\omega \mathcal{E}_{\alpha\beta}(\omega, \mu_F) \hat{\sigma}_{\alpha\beta}(z/\omega, \tau, l_F), \\
\sigma_{pp'}(z, \tau) &= \sum_{\alpha, \beta \in \{q, \bar{q}, g\}} \sigma_{\alpha\beta}(z, \tau, l_F), \quad p' \in \{p, \bar{p}\}, \\
\mathcal{E}_{\alpha\beta}(\omega, \mu_F) &\equiv \int_\omega^1 \frac{dy}{y} [\phi_{\alpha/p}(y, \mu_F) \phi_{\beta/p'}(\omega/y, \mu_F)].
\end{aligned} \tag{3}$$

Note that the $\sigma_{\alpha\beta}$ depend on the factorization scheme (we use $\overline{\text{MS}}$ throughout this paper); only their sum $\sigma_{pp'}$ is physical and thus formally independent of the factorization scale. Nevertheless, it will be useful to study the individual contributions to the total cross section separately as they have very different characteristics. The $\mathcal{E}_{\alpha\beta}$ are parton luminosities and will be discussed in more detail in Section 3.1.

We write the top quark induced partonic cross section as

$$\hat{\sigma}_{\alpha\beta}(x, \tau, l_F) = \sigma_0(\tau) \Delta_{\alpha\beta}(x, \tau, l_F), \tag{4}$$

with

$$\sigma_0(\tau) = \frac{\pi\sqrt{2}G_F}{256} \left(\frac{\alpha_s}{\pi}\right)^2 \tau^2 \left| 1 + (1 - \tau) \arcsin^2 \frac{1}{\sqrt{\tau}} \right|^2, \tag{5}$$

where $G_F \approx 1.16637 \cdot 10^{-5} \text{ GeV}^{-2}$ is Fermi's constant. The kinetic terms assume the form

$$\Delta_{\alpha\beta}(x, \tau, l_F) = \delta_{\alpha g} \delta_{\beta g} \delta(1 - x) + \sum_{n \geq 1} \left(\frac{\alpha_s}{\pi}\right)^n \Delta_{\alpha\beta}^{(n)}(x, \tau, l_F, l_R). \tag{6}$$

At NLO, the full M_t dependence is known in numerical form [4] (the virtual terms are known analytically [18, 19, 20]).

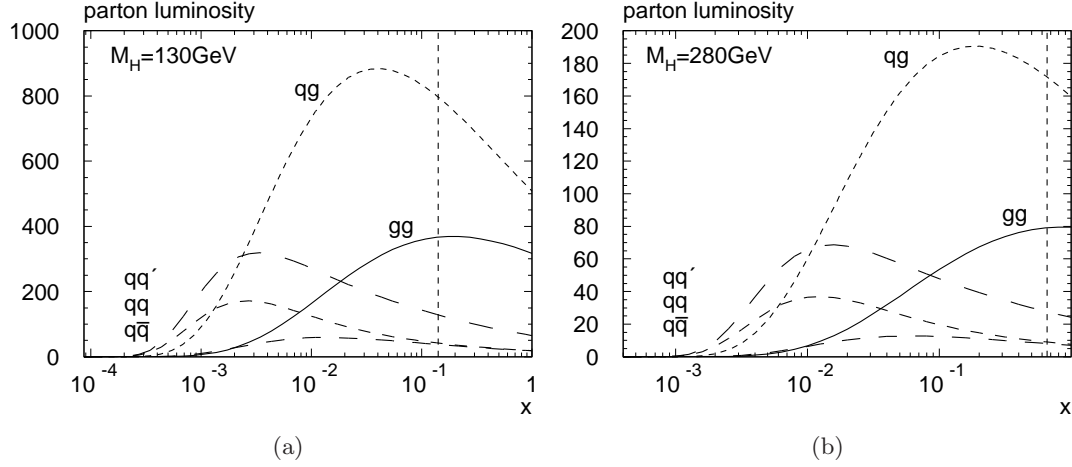


Figure 1: Parton luminosities $\mathcal{E}(\omega = z/x)$ at the LHC for $M_t = 170.9 \text{ GeV}$ at (a) $M_H = 130 \text{ GeV}$ and (b) $M_H = 280 \text{ GeV}$, plotted as functions of $x = M_H^2/\hat{s}$. The vertical line denotes the threshold $\hat{s} = 4M_t^2$.

A fully general result for the partonic cross section at NNLO is as of yet unknown. In Refs. [13, 14, 15, 16], it was evaluated in terms of an expansion of the form

$$\Delta_{\alpha\beta}(x, \tau, \mu_F) = \sum_{i \geq 0} \left(\frac{M_H^2}{M_t^2} \right)^i \Omega_{\alpha\beta,i}(x, l_t, \mu_F), \quad (7)$$

with the analogous perturbative expansion as in Eq. (6). At NNLO, the first four terms ($i \leq 3$) have been evaluated [13, 14]. The so-called EFT approach which has been used in all higher order analyses up to now, can be derived from the leading term of this expansion:

$$\begin{aligned} \sigma_{pp',\infty}(z, l_t) &\equiv \sum_{\alpha,\beta \in \{q,\bar{q},g\}} \int_z^1 d\omega \mathcal{E}_{\alpha\beta}(\omega, \mu_F) \hat{\sigma}_{\alpha\beta,\infty}(z/\omega, l_t, l_F), \\ \hat{\sigma}_{\alpha\beta,\infty}(x, l_t, l_F) &\equiv \sigma_0(\tau) \Omega_{\alpha\beta,0}(x, l_t, l_F), \end{aligned} \quad (8)$$

where σ_0 is given in Eq. (5).

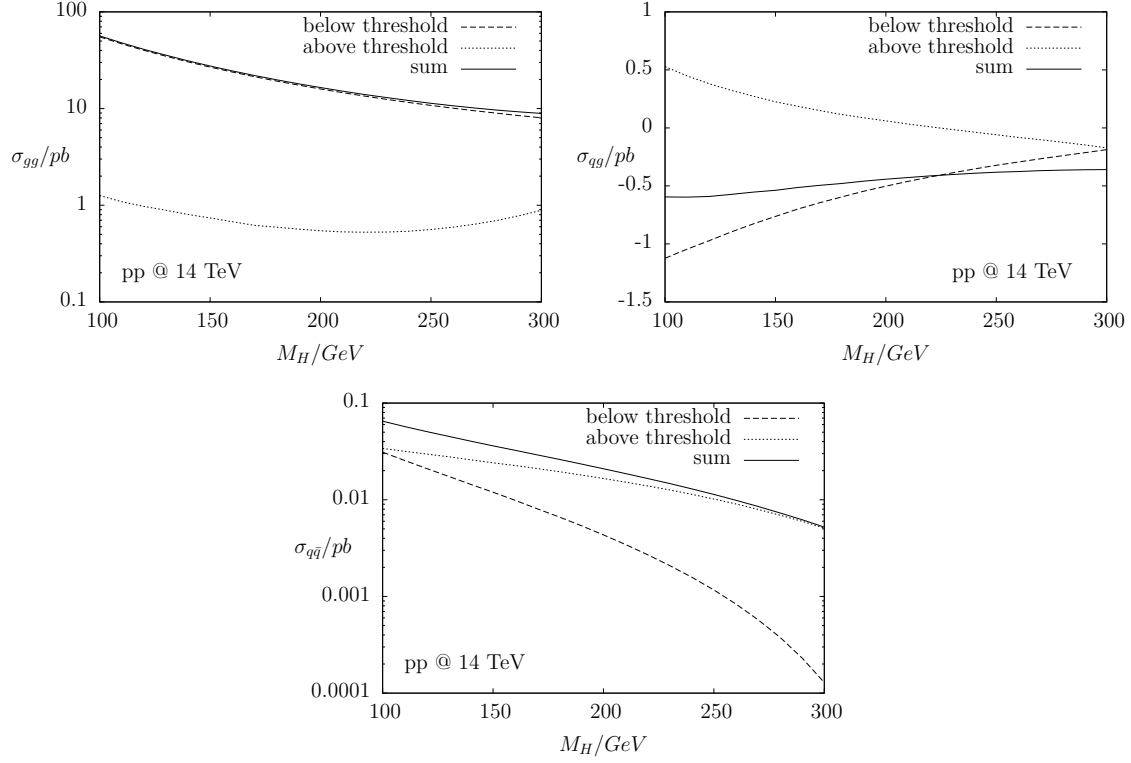


Figure 2: Contributions of the partonic to the hadronic cross section from below ($\hat{s} < 4M_t^2$; dashed) and above ($\hat{s} > 4M_t^2$; dotted) threshold, for the gg , qg , and the $q\bar{q}$ channel at NLO (gg includes the LO contribution). Note that qg uses a linear scale, while for the gg and the $q\bar{q}$ it is logarithmic.

3 Large- \hat{s} limit

3.1 Outline of the problem

The expansion of Eq. (7) is expected to converge within $\hat{s}, M_{\text{H}}^2 \lesssim 4M_t^2$. While the Higgs mass range implied by electro-weak precision measurements lies comfortably in this range, the partonic center-of-mass energy $\sqrt{\hat{s}}$ reaches values far beyond it, both at the LHC and the Tevatron. The corresponding breakdown of convergence manifests itself in inverse powers of $x = M_{\text{H}}^2/\hat{s}$, arising from

$$\frac{\hat{s}}{M_t^2} = \frac{M_{\text{H}}^2}{M_t^2} \cdot \frac{1}{x}. \quad (9)$$

Thus, in general,

$$\Omega_{\alpha\beta,i} \sim \frac{1}{x^i} \quad \text{as } x \rightarrow 0. \quad (10)$$

Note, however, that at small $x = M_{\text{H}}^2/\hat{s}$ there is a strong suppression by the parton luminosity $\mathcal{E}_{\alpha\beta}$ of Eq. (3) which we display for the various sub-channels in Fig. 1. This, together with the fact that $\Omega_{\alpha\beta,0}$ has no power singularities as $x \rightarrow 0$, are the main reasons that the heavy-top limit defined in Eq. (8) works so well.

A further illustration of this observation is shown in Fig. 2 which compares the contributions to the hadronic cross section arising from below ($\hat{s} \leq 4M_t^2$) and above threshold for the various subchannels at NLO. For the dominant gg channel, the region above threshold contributes only of the order of 2%.

However, the spurious $1/x$ singularities described before imply that in order to improve on the heavy-top limit by including higher terms in $1/M_t$, one needs to incorporate information on the large- \hat{s} region. Fortunately, the leading terms can be obtained from general considerations. In the case of the dominant gg -channel, this was done in Ref. [17]. This result was then combined with the $1/M_t$ expansion in Refs. [13, 15].

Considering Fig. 1, it appears that the center of the qg luminosity is at significantly lower values of $x = M_{\text{H}}^2/\hat{s}$ than for gg . Correspondingly, the influence of the region above threshold is larger, as can also be seen in Fig. 2. The proper treatment of this region is thus much more relevant in the qg case. In addition, it is clear *a priori* that the EFT approach, which assumes that the top mass dependence at higher orders is determined by the LO one, cannot work as well in the qg channel which occurs only at NLO. In fact, the contribution of the qg channel to the total cross section in the EFT differs from the exact result by roughly a factor of two in the mass range between $M_{\text{H}} = 100$ and 300 GeV [8].

In the next section, we extend the analysis of Ref. [17] to the qg and pure quark channels ($q\bar{q}$, qq , qq') at NLO and NNLO. The combination with the results of the $1/M_t$ expansion is done in Section 3.3.

3.2 Derivation of the leading high-energy behaviour

The procedure to compute the leading logarithmic behaviour (LL x) of the partonic coefficient function to all orders in the strong coupling α_s is based on k_T -factorization [21]. This technique has been used to resum coefficient functions for a few processes, e.g. heavy quark production [22, 23], deep inelastic scattering [24], Drell-Yan processes [25] and direct photon production [26]. The small x behaviour of Higgs production in gluon fusion was first computed in Ref. [27], in the heavy top approximation. The case of finite top mass was considered in Ref. [17], where it was shown that, as expected, the coefficient function has only single high energy logarithms, while double logarithms appear in the effective theory. In Ref. [17], and in the phenomenological analysis of Ref. [28], only the gluon-gluon channel was considered. In the following the small x behaviour of all the other channels is computed, using high energy colour charge relations. For the sake of clarity, we set $\mu_F = \mu_R$ throughout this derivation.

The partonic cross section which enters the k_T -factorization formula is the leading order cross section for the process $gg \rightarrow H$, computed with two incoming off-shell gluons of momenta $k_{1,2}$, with $k_{1,2}^2 = -|\mathbf{k}_{1,2}|^2$, contracted with eikonal polarizations. The impact factor is defined as the triple Mellin transform of the off-shell cross section

$$h(N, \tau, M_1, M_2) = M_1 M_2 \int_0^1 d\zeta \zeta^{N-1} \int_0^\infty d\xi_1 \xi_1^{M_1-1} \int_0^\infty d\xi_2 \xi_2^{M_2-1} \int_0^{2\pi} \frac{d\varphi}{2\pi} \quad (11)$$

$$M_H^2 \sigma^{\text{off}}(\zeta, \tau, \xi_1, \xi_2, \varphi),$$

where

$$\xi_i = \frac{|\mathbf{k}_i|^2}{M_H^2}, \quad \zeta = \frac{M_H^2}{2(k_1 \cdot k_2 - \mathbf{k}_1 \cdot \mathbf{k}_2)} \quad (12)$$

and φ is the angle between the transverse polarization vectors \mathbf{k}_1 and \mathbf{k}_2 . In Mellin space the high energy limit corresponds to $N \rightarrow 0$; moreover it is easy to see that $M_i \rightarrow 0$ is the collinear limit. The leading high energy behaviour of the coefficient function in the gluon-gluon channel is then found by identifying

$$M_1 = M_2 = \gamma_s \left(\frac{\alpha_s}{N} \right), \quad (13)$$

where γ_s is the anomalous dimension which is dual to the LO BFKL kernel χ_0 , i.e.

$$\chi_0(\gamma_s(\alpha_s/N)) = \frac{N}{\alpha_s}, \quad (14)$$

$$\gamma_s \left(\frac{\alpha_s}{N} \right) = \sum_{k=1}^{\infty} c_k \left(\frac{C_A \alpha_s}{\pi N} \right)^k, \quad c_k = 1, 0, 0, 2\zeta(3), \dots \quad (15)$$

To all orders in perturbation theory, the leading logarithmic contribution to the $\overline{\text{MS}}$ coefficient function is

$$\Delta_{gg}(N, \tau, \mu_F) = h(0, \tau, \gamma_s, \gamma_s) R^2(\gamma_s) \left(\frac{M_H^2}{\mu_F^2} \right)^{2\gamma_s}. \quad (16)$$

The factor R is a scheme dependent function, first computed for $\overline{\text{MS}}$ in [24]. A recent calculation [29] has questioned that result. Although this issue must be solved for the resummation of the small x logarithms, it is not relevant for our present discussion. Our target is to compute the LL x behaviour of the coefficient function through NNLO, but the scheme dependence starts only one order higher:

$$R = 1 + \mathcal{O} \left(\left(\frac{\alpha_s}{N} \right)^3 \right). \quad (17)$$

The high energy behaviour of the other partonic channels can be derived from the gluon-gluon one by noticing that at LL x we have

$$\gamma_{gg} \sim \gamma_s, \quad \gamma_{gq} \sim \frac{C_F}{C_A} \gamma_s, \quad \gamma_{qq} \sim \gamma_{qg} \sim 0. \quad (18)$$

This means that, at LL x , a quark may turn into a gluon, but, because γ_{qg} is next-to-LL x , a gluon cannot turn into a quark. This leads to the following relations between the partonic coefficient functions and the gluonic impact factor [24]:

$$\begin{aligned} \Delta_{qg}(N, \tau, \mu_F) &= \frac{C_F}{C_A} \left[h(0, \tau, \gamma_s, \gamma_s) R^2(\gamma_s) \left(\frac{M_H^2}{\mu_F^2} \right)^{2\gamma_s} \right. \\ &\quad \left. - h(0, \tau, \gamma_s, 0) R(\gamma_s) \left(\frac{M_H^2}{\mu_F^2} \right)^{\gamma_s} \right], \end{aligned} \quad (19)$$

$$\begin{aligned} \Delta_{qq}(N, \tau, \mu_F) &= \left(\frac{C_F}{C_A} \right)^2 \left[h(0, \tau, \gamma_s, \gamma_s) R^2(\gamma_s) \left(\frac{M_H^2}{\mu_F^2} \right)^{2\gamma_s} \right. \\ &\quad \left. - 2h(0, \tau, \gamma_s, 0) R(\gamma_s) \left(\frac{M_H^2}{\mu_F^2} \right)^{\gamma_s} + h(0, \tau, 0, 0) \right]. \end{aligned} \quad (20)$$

Notice that in the high energy limit $\Delta_{qq} = \Delta_{qq'} = \Delta_{q\bar{q}} = \mathcal{O} \left(\frac{\alpha_s^2}{N^2} \right)$, where qq refers to the identical and qq' to the distinct flavour case.

The impact factor can be expanded in powers of M_i , which corresponds to an expansion in powers of α_s :

$$\begin{aligned} h(0, \tau, M_1, M_2) &= M_H^2 \sigma_0(\tau) \left[1 + h^{(1)}(\tau)(M_1 + M_2) \right. \\ &\quad \left. + h^{(2)}(\tau)(M_1^2 + M_2^2) + h^{(1,1)}(\tau)M_1 M_2 + \dots \right] \end{aligned} \quad (21)$$

The coefficients $h^{(1)}$, $h^{(2)}$ and $h^{(1,1)}$ have been evaluated numerically in [17]¹. The only difference here is that, in order to compute the LL x behaviour of all partonic subprocesses, we must keep the contributions $h^{(2)}$ and $h^{(1,1)}$ separated.

It is then easy to substitute Eq. (21) into Eqs. (19), (20) and invert the N Mellin transform to obtain the result in x space. Through NNLO, the small x limit of the partonic coefficient functions can be written as follows:

$$\begin{aligned} \Delta_{gg}(x, \tau) &= \delta(1-x) + \frac{\alpha_s}{\pi} \left[B_{gg}^{(1)}(\tau) - 2C_A l_F + \mathcal{O}(x) \right] \\ &\quad + \left(\frac{\alpha_s}{\pi} \right)^2 \left[\left(A_{gg}^{(2)}(\tau) - 2C_A B_{gg}^{(1)}(\tau) l_F + 2C_A^2 l_F^2 \right) \ln \frac{1}{x} + B_{gg}^{(2)}(\tau) + \mathcal{O}(x) \right], \\ \Delta_{qg}(x, \tau) &= \frac{\alpha_s}{\pi} \left[B_{qg}^{(1)}(\tau) - C_F l_F + \mathcal{O}(x) \right] \\ &\quad + \left(\frac{\alpha_s}{\pi} \right)^2 \left[\left(A_{qg}^{(2)}(\tau) - \frac{3}{2} C_F B_{qg}^{(1)}(\tau) l_F + \frac{3}{2} C_A C_F l_F^2 \right) \ln \frac{1}{x} + B_{qg}^{(2)}(\tau) + \mathcal{O}(x) \right], \\ \Delta_{q\bar{q}}(x, \tau) &= \Delta_{qq}(x, \tau) = \Delta_{q\bar{q}'}(x, \tau) = \\ &= \left(\frac{\alpha_s}{\pi} \right)^2 \left[\left(A_{qq}^{(2)}(\tau) - \frac{C_F^2}{C_A} B_{gg}^{(1)}(\tau) l_F + C_F^2 l_F^2 \right) \ln \frac{1}{x} + B_{qq}^{(2)}(\tau) + \mathcal{O}(x) \right]. \end{aligned} \quad (22)$$

Recall that we set $\mu_F = \mu_R$ in this section. The full μ_F , μ_R -dependence is obtained by replacing

$$\alpha_s \rightarrow \alpha_s(\mu_R^2) \left[1 - \frac{\alpha_s(\mu_R^2)}{\pi} \beta_0 l_{\text{FR}} + \left(\frac{\alpha_s(\mu_R^2)}{\pi} \right)^2 ((\beta_0 l_{\text{FR}})^2 - \beta_1 l_{\text{FR}}) \right] \quad (23)$$

in $\sigma_0 \Delta_{\alpha\beta}$, where $l_{\text{FR}} = \ln(\mu_F^2/\mu_R^2)$ and $\beta_0 = 23/12$, $\beta_1 = 29/12$.

The coefficients $A_{\alpha\beta}^{(2)}$ and $B_{\alpha\beta}^{(1)}$ are provided in the form of numerical tables in Table 1. For all coefficients, the dependence on τ is very smooth and can safely be interpolated by straight lines, for example. The NNLO constants $B_{\alpha\beta}^{(2)}$ are currently unknown; their influence on the final result will be studied at the end of Section 4.

¹See Eq. (36) and Eq. (38) of that paper, but notice the differences in the notation, e.g. the definition of τ .

τ	$B_{gg}^{(1)}$	$B_{qg}^{(1)}$	τ	$A_{gg}^{(2)}$	$A_{qg}^{(2)}$	$A_{qq}^{(2)}$
1.0	-0.8821	-0.1960	1.0	33.0465	8.7703	1.2681
1.5	2.9212	0.6492	1.5	35.9907	9.5484	1.3782
2.0	5.0234	1.1163	2.0	44.2884	12.2677	2.1563
2.5	6.5538	1.4564	2.5	53.1336	15.1924	3.0088
3.0	7.7650	1.7255	3.0	61.8029	18.0679	3.8524
3.5	8.7693	1.9487	3.5	70.1088	20.8272	4.6644
4.0	9.6279	2.1395	4.0	78.0127	23.4553	5.4393
4.5	10.3781	2.3062	4.5	85.5245	25.9547	6.1771
5.0	11.0444	2.4543	5.0	92.6698	28.3331	6.8798
5.5	11.6437	2.5875	5.5	99.4782	30.6002	7.5501
6.0	12.1883	2.7085	6.0	105.9788	32.7654	8.1907
6.5	12.6875	2.8194	6.5	112.1985	34.8374	8.8039
7.0	13.1482	2.9218	7.0	118.1616	36.8244	9.3922
7.5	13.5760	3.0169	7.5	123.8897	38.7333	9.9576
8.0	13.9752	3.1056	8.0	129.4021	40.5706	10.5019
8.5	14.3495	3.1888	8.5	134.7158	42.3420	11.0268
9.0	14.7018	3.2671	9.0	139.8461	44.0524	11.5337
9.5	15.0345	3.3410	9.5	144.8064	45.7063	12.0240
10.0	15.3497	3.4110	10.0	149.6090	47.3077	12.4989
10.5	15.6491	3.4776	10.5	154.2646	48.8603	12.9594
11.0	15.9343	3.5410	11.0	158.7829	50.3672	13.4064
11.5	16.2065	3.6015	11.5	163.1728	51.8315	13.8408
12.0	16.4670	3.6593	12.0	167.4422	53.2556	14.2633

Table 1: Coefficients for the large- \hat{s} behaviour at NLO (left table) and NNLO (right).

3.3 Merging and partonic results

Let us recall the knowledge of the partonic cross section at NNLO. Below threshold ($\hat{s} < 4M_t^2$), the result is known in terms of an expansion in $1/M_t$ and $(1-x)$ [13, 15, 14]². Both expansions are expected to converge very well as long as $M_H < 2M_t \approx 340$ GeV. This is indeed observed for the gg and the $q\bar{q}$ channels at NLO in Fig. 3 for $M_H = 130$ GeV and in Fig. 4 for $M_H = 280$ GeV. They show the partonic cross sections below threshold, keeping terms of order $(1-x)^a(1/M_t^2)^b$. In the left columns, $a = 0, \dots, 8$ and $b = 5$ (long to short dashes), while in the right columns, $a = 8$ and $b = 0, \dots, 5$. These figures compare the expansions to the exact result which we derived using standard techniques (see, e.g., Ref. [30]). In fact, the behaviour of the expansions suggests that, below threshold, the final result for the gg and the $q\bar{q}$ channels is numerically almost equivalent to the full M_t and x dependence.

The NLO $q\bar{q}$ channel, on the other hand, has a very peculiar structure at threshold. At this order only one diagram with $q\bar{q}$ annihilating into an s -channel gluon contributes. Such a diagram is not enhanced in either the large- or small- x region, leaving room for a relatively pronounced structure at the threshold which cannot be described properly in our approach. However, the contribution of the $q\bar{q}$ channel to the hadronic cross section is down by almost three orders of magnitude relative to the gg channel, and still a factor of ten relative to the qg channel. We will nevertheless investigate its influence on the final prediction in more detail below. At higher orders we expect this effect to be reduced, because other diagrams with non-trivial high- or low- x limits will contribute.

The corresponding curves at NNLO are shown in Figs. 5–8. There is no exact result that one could compare to, but the quality of the convergence both of the $1/M_t$ and the $(1-x)$ expansions below threshold convincingly shows that they approximate the exact result to a very high degree in this region.

From Section 3.2 we know the leading high energy behaviour for general values of M_t and M_H . There are many ways then to merge the available information into a smooth function with the correct high- and low-energy behaviour (see, e.g., Refs. [17, 28, 15]). We decide to use [13]

$$\begin{aligned} \hat{\sigma}_{\alpha\beta}^{(n)}(x) = & \hat{\sigma}_{\alpha\beta,N}^{(n)}(x) + \sigma_0 A_{\alpha\beta}^{(n)} \left[\ln \frac{1}{x} - \sum_{k=1}^N \frac{1}{k} (1-x)^k \right] \\ & + (1-x)^{N+1} \left[\sigma_0 B_{\alpha\beta}^{(n)} - \hat{\sigma}_{\alpha\beta,N}^{(n)}(0) \right], \end{aligned} \quad (24)$$

where $\hat{\sigma}_{\alpha\beta,N}^{(n)}(x)$ denotes the soft expansion of the partonic cross section through order

²Recently, the full x dependence was derived [16]. However, as argued before, the x dependence of the $1/M_t$ expansion does not hold for $x < M_H^2/(4M_t^2)$.

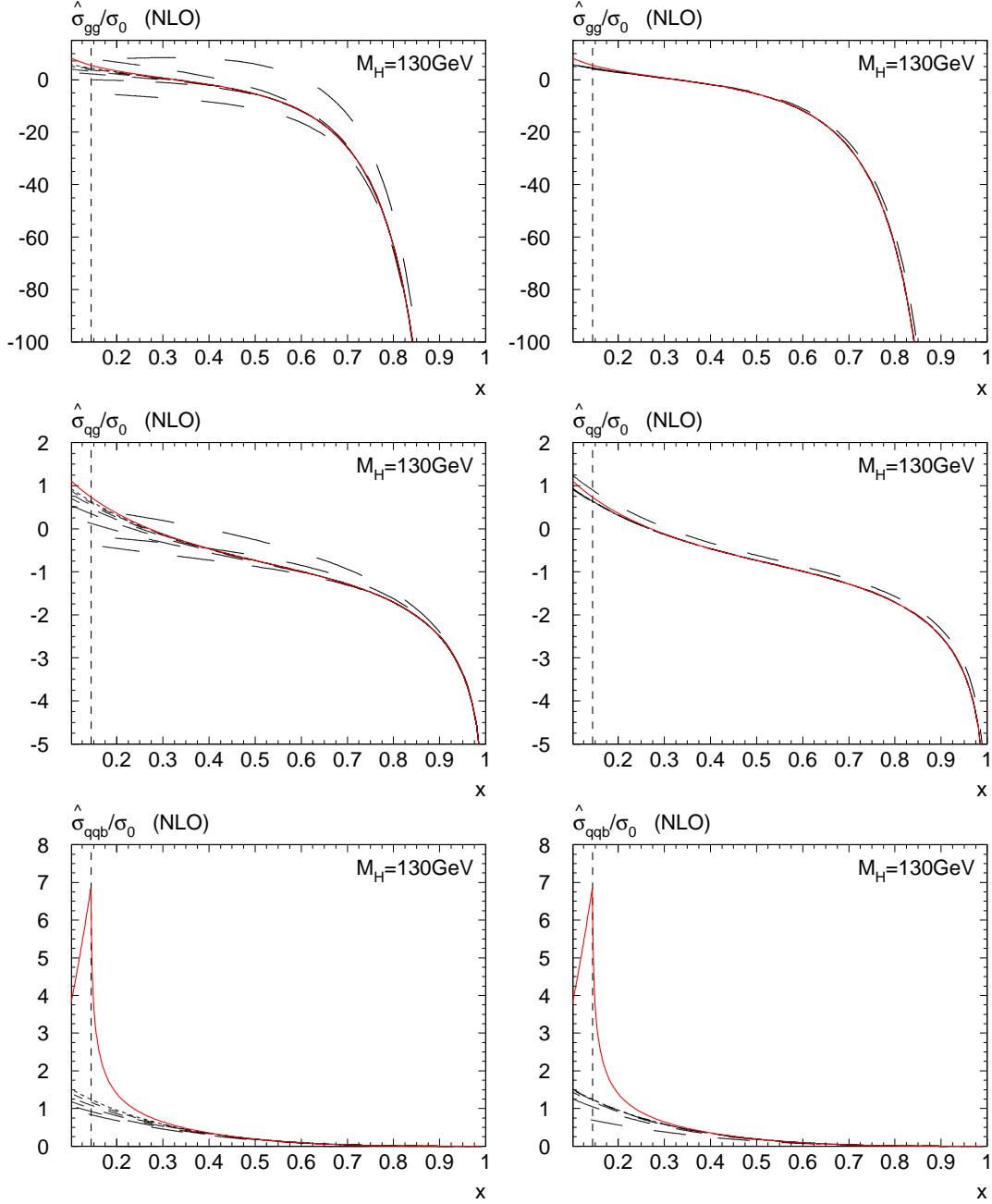


Figure 3: Partonic cross section at NLO for $M_t = 170.9$ and $M_H = 130$ GeV at various orders in the expansion parameters (increasing order corresponds to decreasing dash size of the lines). Left column: $\mathcal{O}(1/M_t^{10})$ and $\mathcal{O}((1-x)^n)$, $n = 0, \dots, 8$. Right column: $\mathcal{O}((1-x)^8)$ and $\mathcal{O}(1/M_t^{2n})$, $n = 0, \dots, 5$. Solid: exact. The dashed vertical line indicates the threshold.

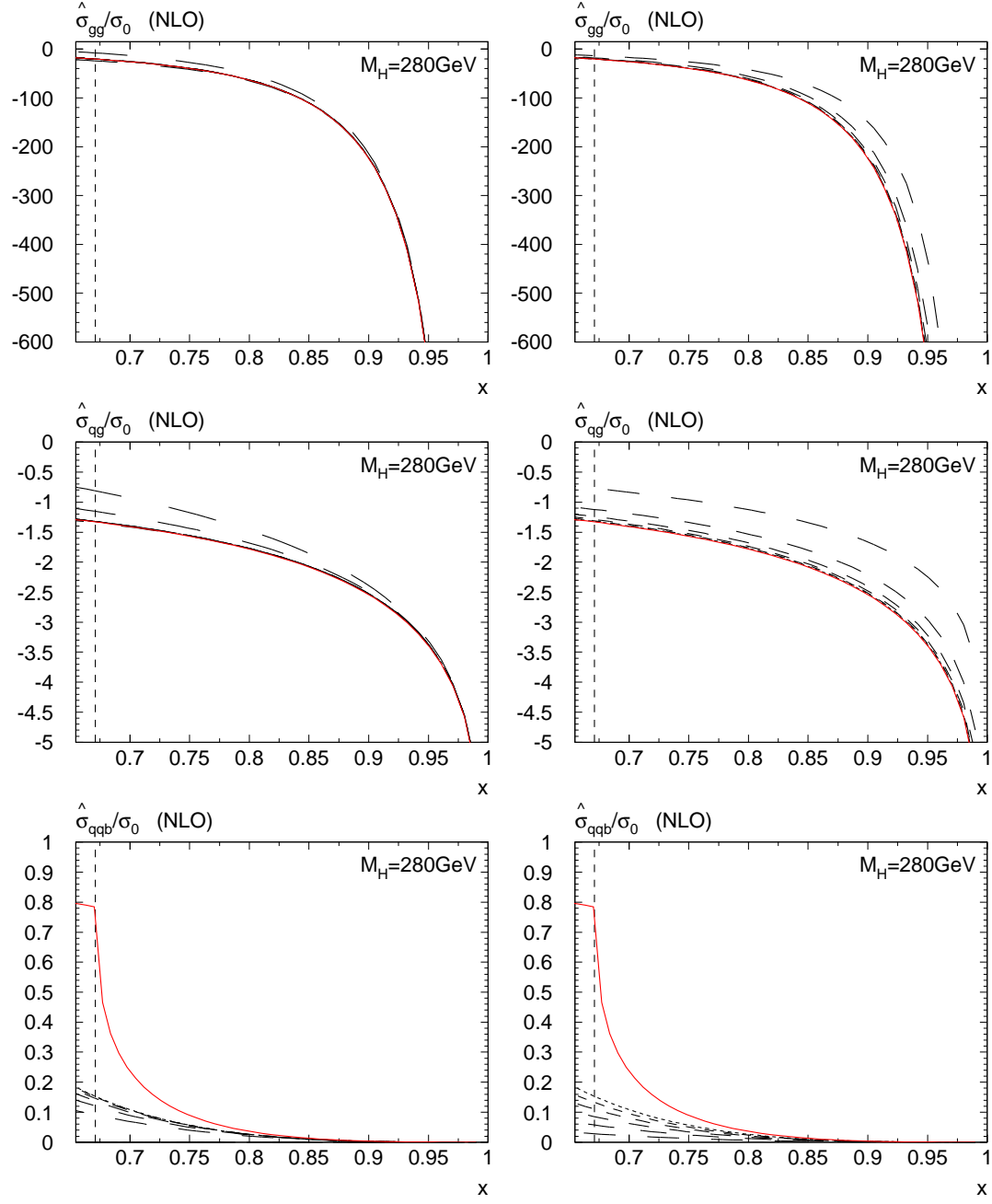


Figure 4: Same as Fig. 3, but for $M_H = 280 \text{ GeV}$.

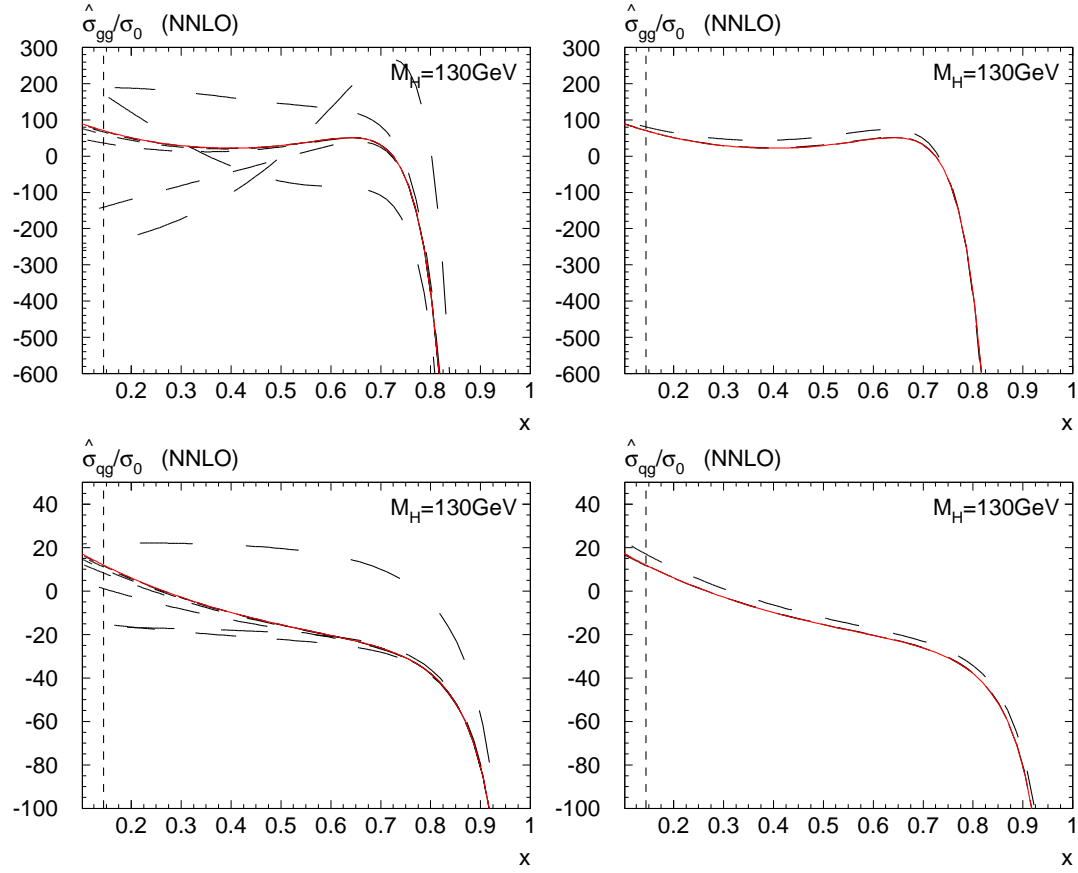


Figure 5: Partonic cross section (gg and qq channel) at NNLO for $M_t = 170.9$ and $M_H = 130$ GeV for various orders in the expansion parameters (increasing order corresponds to decreasing dash size of the lines). Left column: $\mathcal{O}(1/M_t^{10})$ and $\mathcal{O}((1-x)^n)$, $n = 0, \dots, 7$. Right column: $\mathcal{O}((1-x)^8)$ and $\mathcal{O}(1/M_t^{2n})$, $n = 0, \dots, 2$. Solid: $\mathcal{O}(1/M_t^6)$ and $\mathcal{O}((1-x)^8)$. The dashed vertical line indicates the threshold. For the $q\bar{q}$ and the qq channel, see Fig. 6.

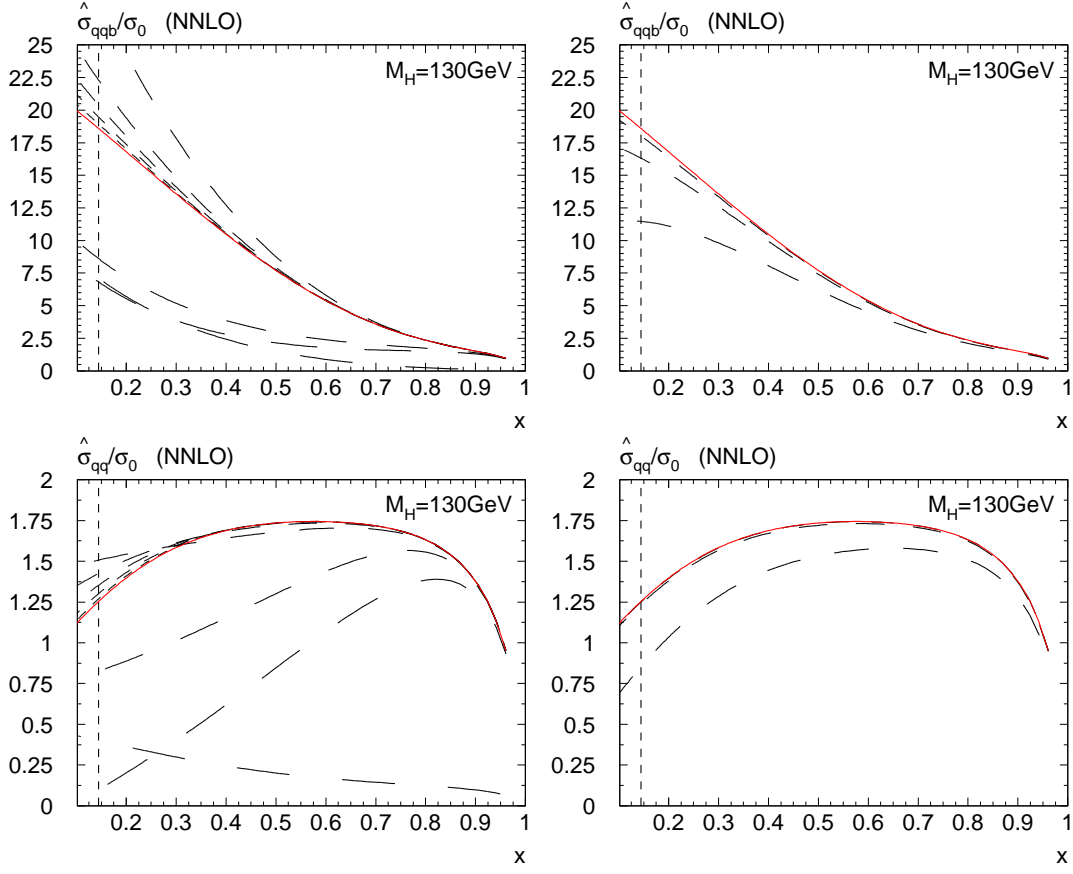


Figure 6: Same as Fig. 5, but for the $q\bar{q}$ and the qq channels (identical quark flavors). The figure for the qq' channel (different quark flavours) is not shown since it is almost indistinguishable from the one for qq .

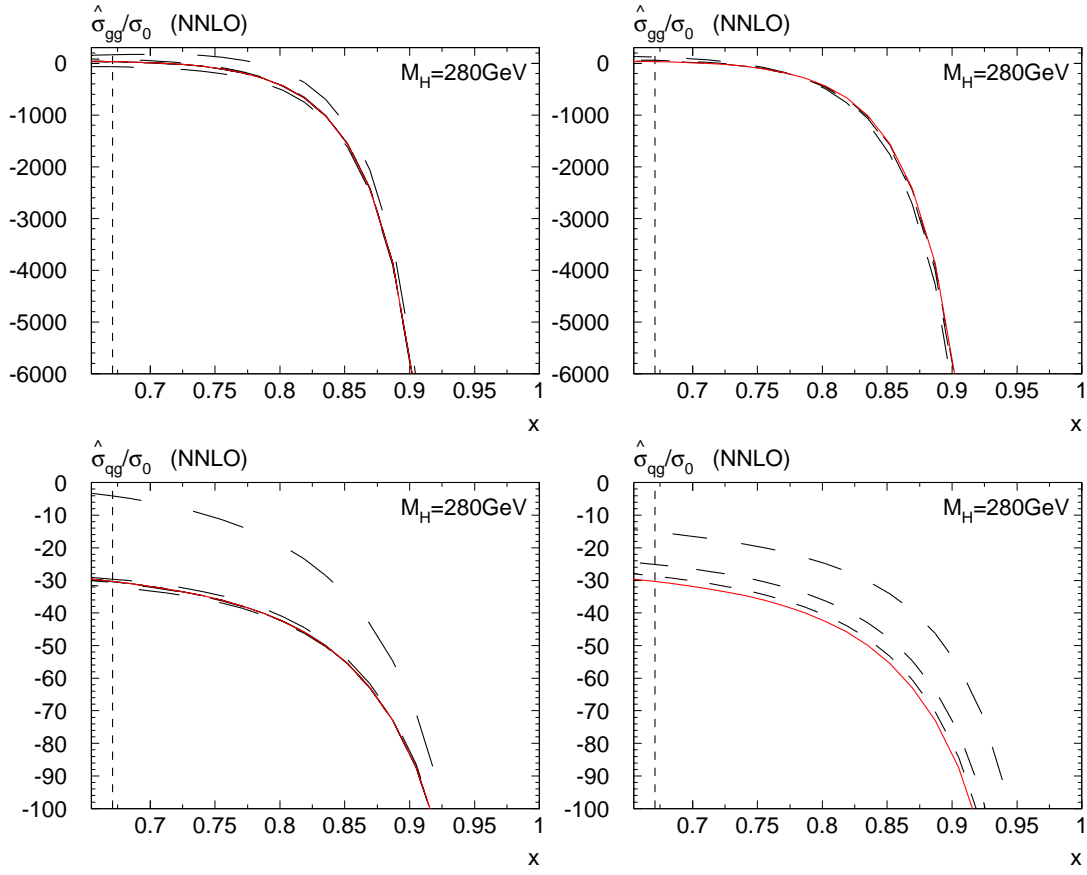


Figure 7: Same as Fig. 5, but for $M_H = 280 \text{ GeV}$.

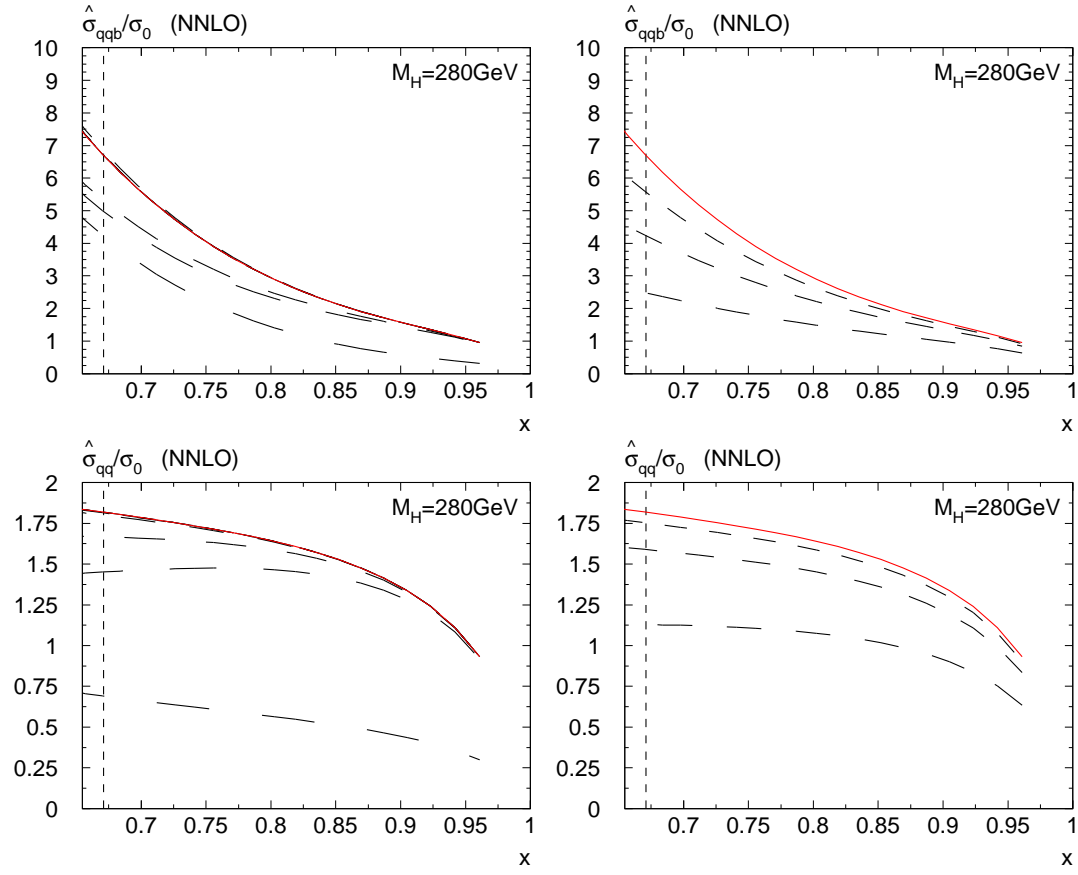


Figure 8: Same as Fig. 6, but for $M_H = 280 \text{ GeV}$.

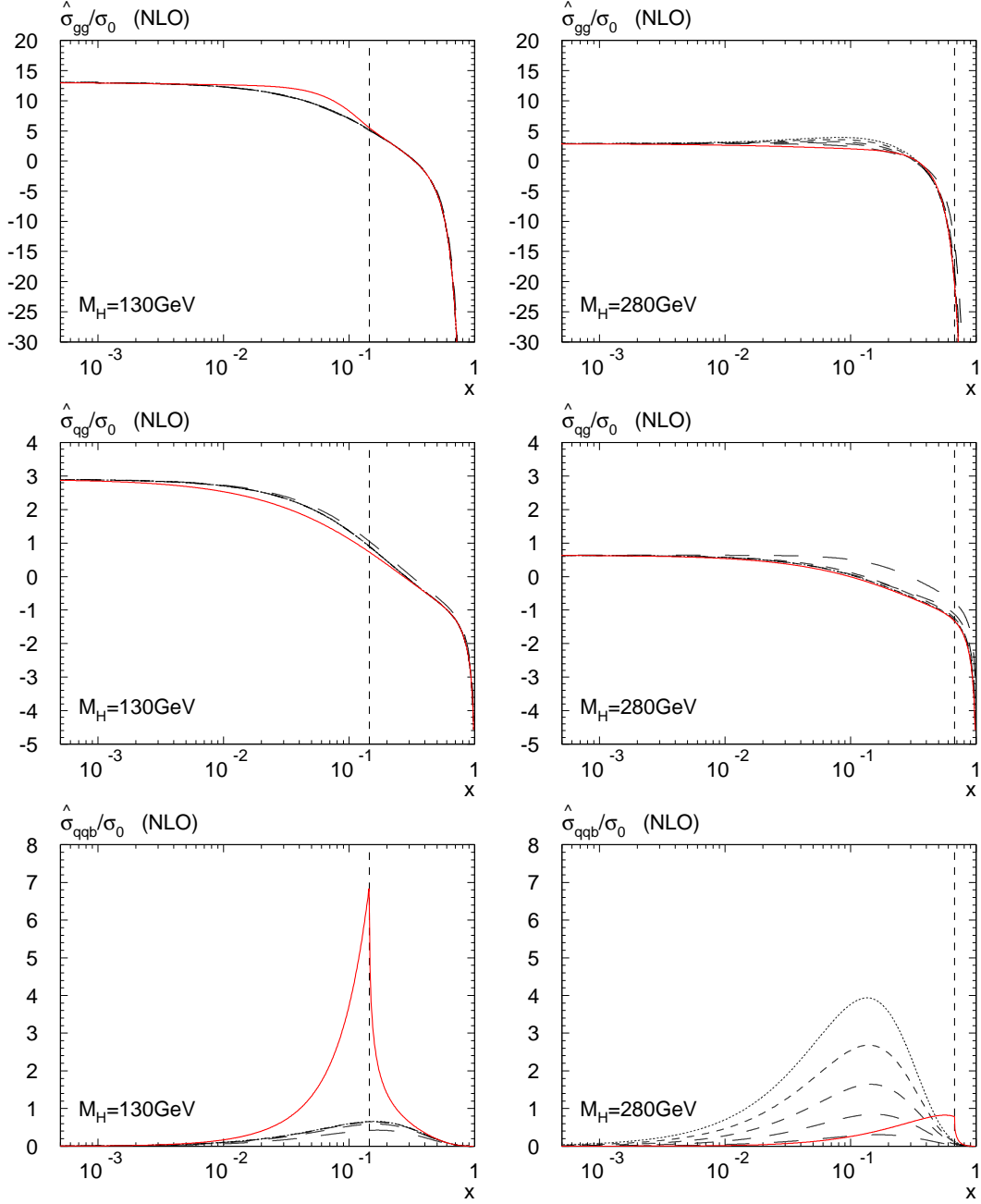


Figure 9: NLO partonic cross sections as constructed from Eq. (24) (with $N = 8$) by including successively higher orders in $1/M_t^2$. Dashed: $\mathcal{O}(M_t^{2n})$, $n = 0, \dots, 5$. Solid: exact. Left/right column: $M_H = 130 \text{ GeV}/M_H = 280 \text{ GeV}$. The dashed vertical line indicates the threshold.

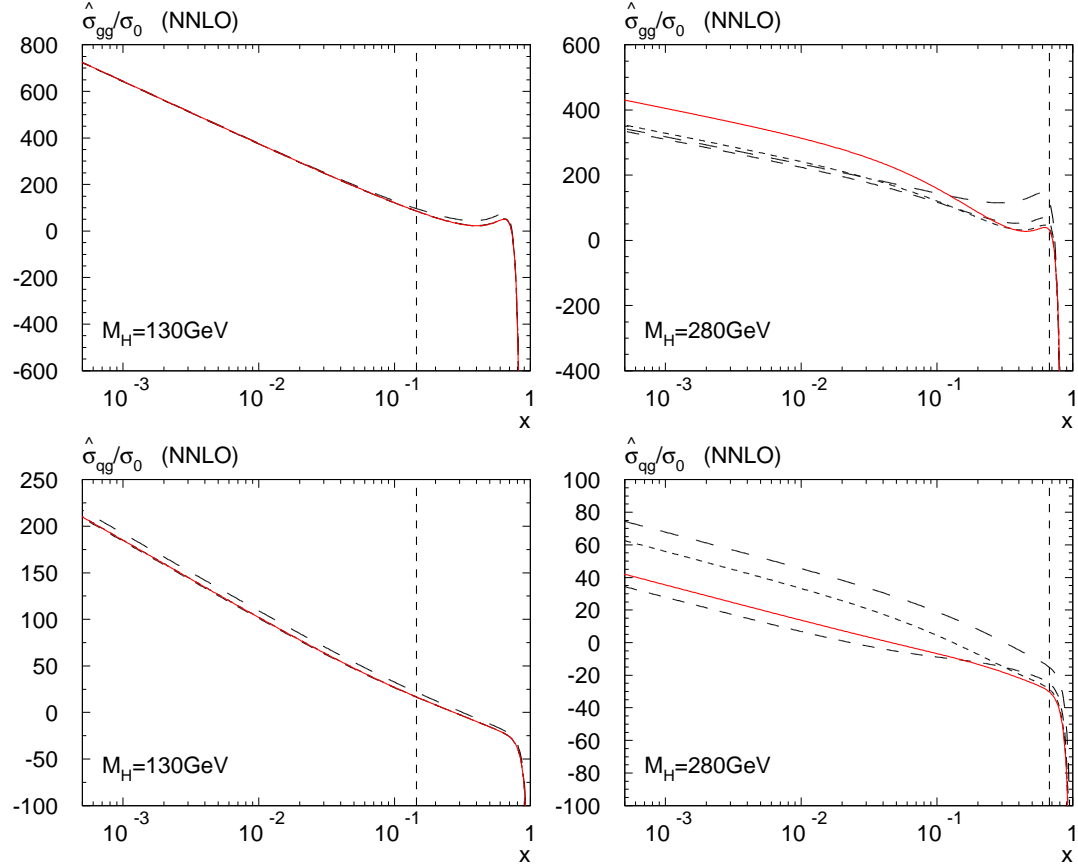


Figure 10: NNLO partonic cross sections (gg and qq channel) as constructed from Eq. (24) (with $N = 8$) by including successively higher orders in $1/M_t^2$. Dashed: $\mathcal{O}(M_t^{2n})$, $n = 0, 1, 2$. Solid: $n = 3$. Left/right column: $M_H = 130 \text{ GeV}/M_H = 280 \text{ GeV}$. The dashed vertical line indicates the threshold. For the $q\bar{q}$ and the qq channel, see Fig. 11.

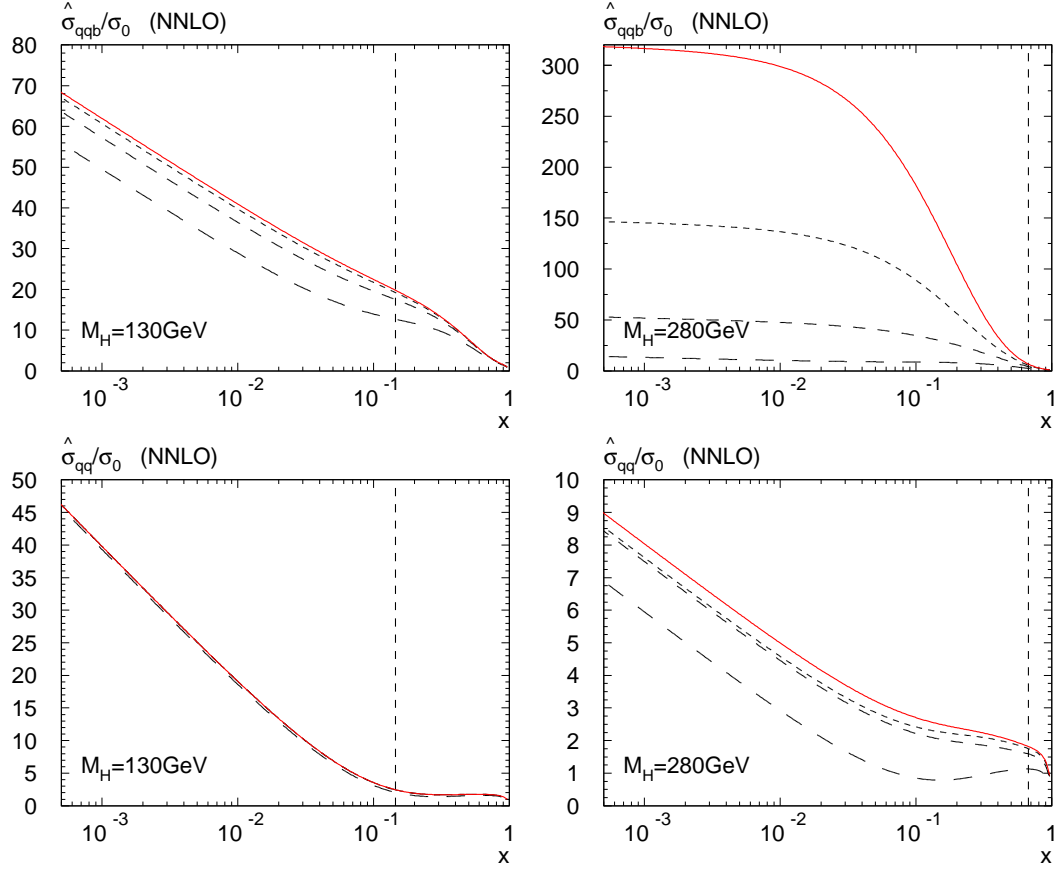


Figure 11: Same as Fig. 10, but for the $q\bar{q}$ and the qq channels (identical quark flavors). The figure for the qq' channel (different quark flavours) is not shown since it is almost indistinguishable from the one for qq .

$(1-x)^N$. For the unknown constants at NNLO we use the default values $\sigma_0 B_{\alpha\beta}^{(2)} = \hat{\sigma}_{\alpha\beta,N}^{(n)}(0)$, but we will study their influence on the NNLO hadronic results at the end of Section 4.

At NLO, the resulting partonic cross sections are shown in Fig. 9 for $M_H = 130$ GeV and $M_H = 280$ GeV. The precision to which the gg and qg channels reproduce the exact result is quite impressive. As expected, the $q\bar{q}$ channel is approximated only very poorly though.

The corresponding plots at NNLO are shown in Fig. 10 and 11, for the default values of the high energy constant $B_{\alpha\beta}^{(2)}$. Note that due to this undetermined constant, the curves do not all converge to the same point for $x \rightarrow 0$ as is the case at NLO. Only the slope is determined by the logarithmic coefficient $A_{\alpha\beta}^{(2)}$. Nevertheless, convergence for the gg and the qg channel is very good, in particular at low Higgs masses. At larger Higgs masses, the x dependence becomes more and more unreliable as more terms in $1/M_t$ are included. This leads to the observed variations of the final result at $M_H = 280$ GeV. As will be shown at the end of Section 4, however, the variations affect the hadronic cross section by less than 1%.

As expected, the $q\bar{q}$ channel does not seem to converge, but its contribution to the hadronic cross section is negligible as are those of the qg and the $q\bar{q}'$ channels (equal and different quark flavours, respectively). The observed convergence of the latter is much better though. In the following, we will include them in the total hadronic cross section, but we will only discuss the $q\bar{q}$ channel as representative of the pure quark channels (the one with the worst convergence behaviour).

4 Hadronic Results

In order to study the effect of the $1/M_t$ terms on the hadronic cross section, we define (see also Ref. [13])

$$\begin{aligned}\hat{\sigma}_{\alpha\beta}^{\text{NLO}}(M_t^n) &= \sigma_0 \delta_{\alpha g} \delta_{\beta g} \delta(1-x) + \hat{\sigma}_{\alpha\beta}^{(1)}(M_t^n), \\ \hat{\sigma}_{\alpha\beta}^{\text{NNLO}}(M_t^n) &= \sigma_0 \left[\delta_{\alpha g} \delta_{\beta g} \delta(1-x) + \Delta_{\alpha\beta,\infty}^{(1)} \right] + \hat{\sigma}_{\alpha\beta}^{(2)}(M_t^n),\end{aligned}\tag{25}$$

where $\hat{\sigma}_{\alpha\beta}^{(k)}(M_t^n)$ is the N^kLO contribution to the partonic cross section evaluated as an expansion through $\mathcal{O}(1/M_t^n)$, and matched to the low- x limit as described in Section 3.2. $\Delta_{\alpha\beta,\infty}^{(1)}$ is the EFT result as defined in Eq. (8). Note that this differs from an *extended* EFT *approach*, where $\Delta_{\alpha\beta}^{(k)}$ would be expanded in terms of $1/M_t$, while the full τ dependence in $\sigma_0(\tau)$ is kept. We will return to this latter approach at the end of this section. The corresponding hadronic quantities derived from Eq. (25) are denoted by $\sigma_{\alpha\beta}^{\text{NLO}}(M_t^n)$ and $\sigma_{\alpha\beta}^{\text{NNLO}}(M_t^n)$.

Fig. 12 shows the relative gg , qg and $q\bar{q}$ contribution $\sigma_{\alpha\beta}^{\text{NLO}}(M_t^n)$ to the total hadronic cross section. The dashed lines correspond to successively higher orders in $1/M_t$, while the solid line shows the exact result. The curves are all normalized to the exact NLO cross section σ^{NLO} . For the gg and the qg channels, one observes excellent convergence towards the exact result (solid line). The small deviations are reflections of the deviations between the solid and the dashed lines in Fig. 9 (a)-(d). As pointed out above, the mass effects in the qg channel are quite large, ranging from roughly a factor of two to four in the relevant Higgs mass range. Of course, the overall size of the qg channel is below 5%. As expected, the picture in the $q\bar{q}$ channel is significantly worse. Only the order of magnitude is captured, but there is no sign of convergence towards the exact result whatsoever. Its contribution to the total cross section is only of order 10^{-3} though and thus irrelevant.

The corresponding plots at NNLO are shown in Fig. 13. Since there is no exact result in this case, we normalize the curves to the full NNLO EFT result, cf. Eq. (8). Also, the solid lines always refer to the subchannels evaluated in the EFT approach. The observations are quite similar as at NLO: the difference between the EFT result and the $1/M_t$ expansion for the gg channel is about 1% which is of the order of the accuracy to which we expect the capture the mass effects. In the qg channel, the relative difference between the EFT result and the $1/M_t$ expansion is significantly larger ($\sim 20\%$), but the influence of this effect on the total cross section is again only of order 1% due to the strong suppression of the qg channel. The $q\bar{q}$ channel does not seem to converge very well, but is numerically negligible (the true mass effects are not expected to change this).

The hadronic results for the Tevatron are shown in Fig. 14 at NLO and NNLO. The conclusions are very similar to those for the LHC, thus justifying the use of the EFT approximation for Higgs searches also in this case [31].

Overall, we conclude that the final result for the NNLO cross section including top mass effects is within 1% of the EFT result.

Dependence on $B_{\alpha\beta}^{(2)}$. As pointed out above, the constants $B_{\alpha\beta}^{(2)}$ for the large- \hat{s} behaviour are currently unknown. From the curves in Fig. 10 and 11, our choice $\sigma_0 B_{\alpha\beta}^{(2)} = \hat{\sigma}_{\alpha\beta}^{(2)}(0)$ seems to be reasonable, leading to rather smooth curves over the full x -range. Nevertheless, in order to estimate the uncertainty induced by this unknown constant, we set $\sigma_0 B_{gg}^{(2)} = t \times \hat{\sigma}_{gg}^{(2)}(0)$ and find that the dependence of the hadronic cross section on t is very well described by a linear function:

$$\sigma^{\text{NNLO}} \Big|_t \approx (1 - 0.01 t) \sigma^{\text{NNLO}} \quad (26)$$

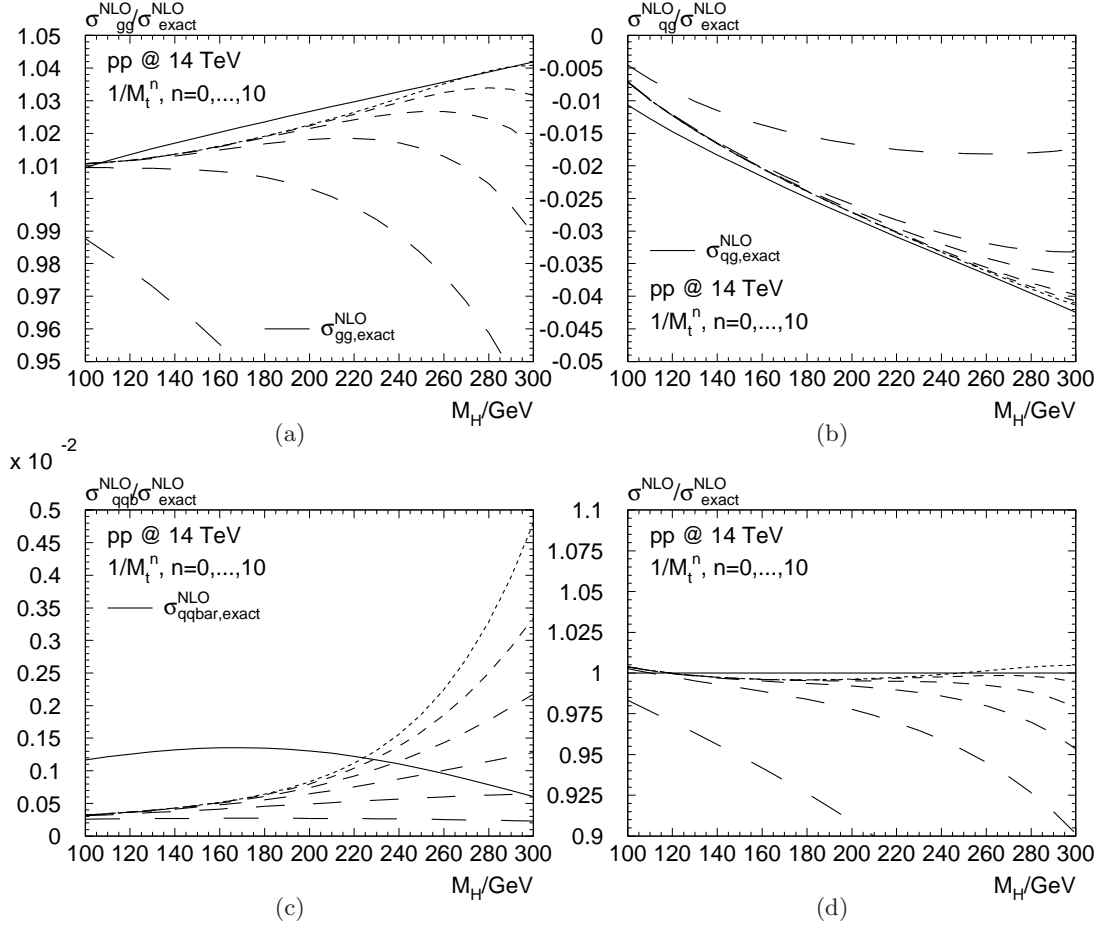


Figure 12: (a)-(c) Sub-channel contributions to the hadronic cross section at NLO, normalized to the full result. Note that gg includes the exact LO contribution, cf. Eq. (25). Dashed: including terms of order $1/M_t^{2n}$ in the numerator ($n = 0, \dots, 5$ from long to short dashes). Solid: exact. (d) Sum over all sub-channels.

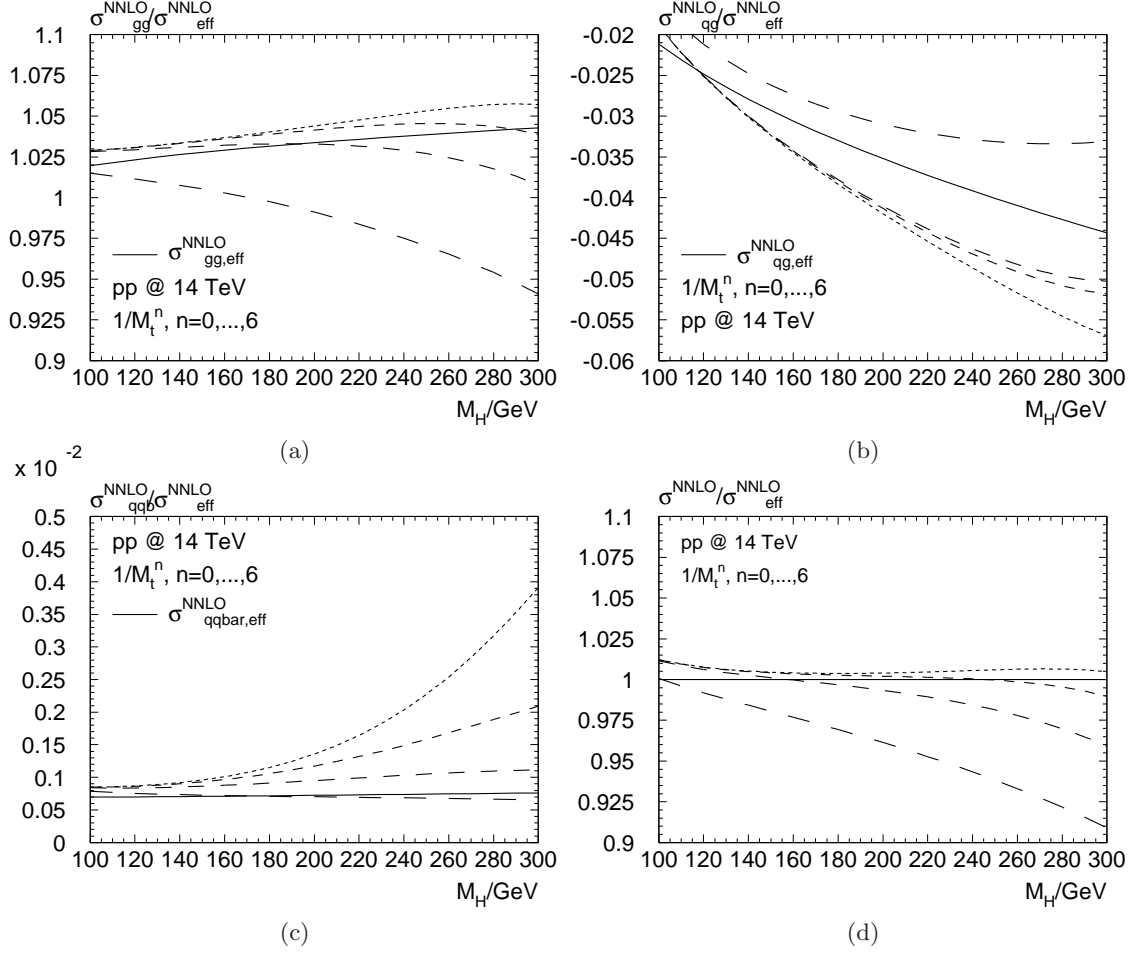


Figure 13: (a)-(c) Sub-channel contributions to the hadronic cross section at NNLO, normalized to the full NNLO EFT result (LHC conditions). Note that all channels include their lower order contributions *in the EFT approach* (cf. Eq.(25)). Dashed: including terms of order $1/M_t^{2n}$ in the numerator ($n = 0, 1, 2, 3$ from long to short dashes). Solid: EFT result. (d) Sum over all sub-channels.

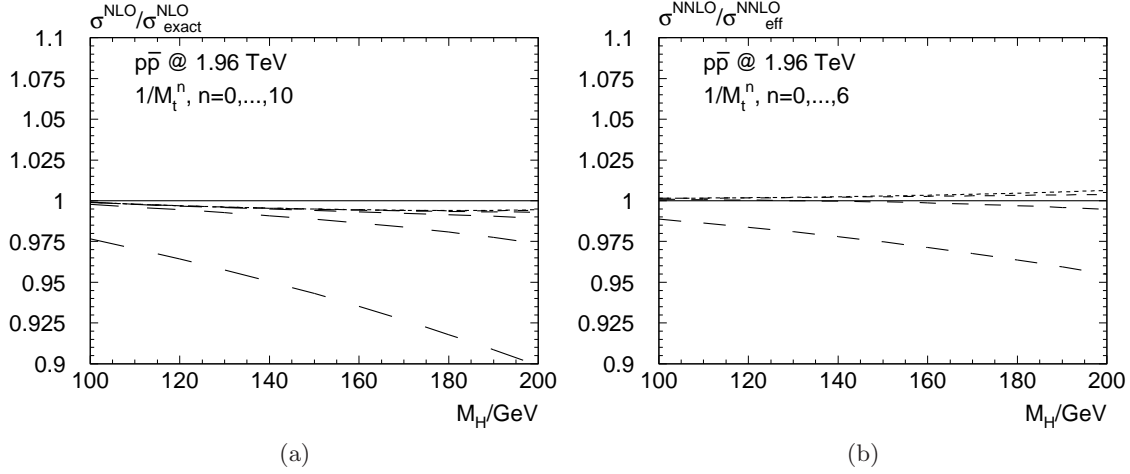


Figure 14: Hadronic cross section at (a) NLO and (b) NNLO for the Tevatron, normalized to the full NNLO EFT result. Note that the lower order contributions are included *in the EFT approach* (cf. Eq. (25)). Dashed: including terms of order $1/M_t^{2n}$ in the numerator ($n = 0, 1, 2, 3$ from long to short dashes). Solid: EFT result.

Again recalling the smoothness of the curves in Fig. 10 and 11, we do not expect the parameter t to be significantly larger than one. The resulting uncertainty is therefore at most at the percent level and therefore much smaller than the scale uncertainty of the NNLO result.

Is the heavy-top limit a coincidence? Let us conclude this section with a remark on the *extended EFT approach* as mentioned in the discussion after Eq. (25). It would be possible that the high quality of the EFT approach is a coincidence, in the sense that there is an accidental cancellation among the higher order terms in the $1/M_t$ expansion of the $\Delta_{\alpha\beta}$. This would have a significant effect on the applicability of the EFT approach to other quantities, of course.

However, we have checked that this is not the case. All the curves of the extended EFT approach lie within 1% of our final result.

5 Conclusions

The hadronic Higgs production cross section due to gluon fusion was presented including effects from a finite top quark mass. We have extended previous analyses by deriving the high-energy limits of all partonic sub-channels and combining them with the known $1/M_t$ expansions. Although the mass effects on the absolute size of the $q\bar{q}$ channel are large, they have no significant effect on the total hadronic cross section. Therefore, the main conclusions of previous analyses [14, 16] remain valid, and the EFT approach is still justified.

Acknowledgments. We would like to thank Stefano Forte for useful comments on the manuscript. This work was supported by DFG contract HA 2990/3-1, and by the *Helmholtz Alliance “Physics at the Terascale”*. SM would like to thank Bergische Universität Wuppertal for the kind hospitality. The work of SM is supported by UK’s STFC.

References

- [1] A. Djouadi, *The anatomy of electro-weak symmetry breaking. I: The Higgs boson in the standard model*, *Phys. Reports* **457** (2008) 1, [hep-ph/0503172](#).
- [2] A. Djouadi, *The anatomy of electro-weak symmetry breaking. II: The Higgs bosons in the minimal supersymmetric model*, *Phys. Reports* **459** (2008) 1, [hep-ph/0503173](#).
- [3] S. Dawson, *Radiative corrections to Higgs boson production*, *Nucl. Phys. B* **359** (1991) 283.
- [4] D. Graudenz, M. Spira, P.M. Zerwas, *QCD corrections to Higgs boson production at proton-proton colliders*, *Phys. Rev. Lett.* **70** (1993) 1372.
- [5] M. Spira, A. Djouadi, D. Graudenz, P.M. Zerwas, *Higgs boson production at the LHC*, *Nucl. Phys. B* **453** (1995) 17, [hep-ph/9504378](#).
- [6] Y. Schröder and M. Steinhauser, *Four-loop decoupling relations for the strong coupling*, *JHEP* **0601** (2006) 051, [hep-ph/0512058](#).
- [7] K.G. Chetyrkin, J.H. Kühn, C. Sturm, *QCD decoupling at four loops*, *Nucl. Phys. B* **744** (2006) 121, [hep-ph/0512060](#).
- [8] M. Spira, *HIGLU: A Program for the Calculation of the Total Higgs Production Cross Section at Hadron Colliders via Gluon Fusion including QCD Corrections*, [hep-ph/9510347](#).

- [9] R.V. Harlander and W.B. Kilgore, *Next-to-next-to-leading order Higgs production at hadron colliders*, *Phys. Rev. Lett.* **88** (2002) 201801, [hep-ph/0201206](#).
- [10] C. Anastasiou and K. Melnikov, *Higgs boson production at hadron colliders in NNLO QCD*, *Nucl. Phys.* **B 646** (2002) 220, [hep-ph/0207004](#).
- [11] V. Ravindran, J. Smith, W.L. van Neerven, *NNLO corrections to the total cross section for Higgs boson production in hadron hadron collisions*, *Nucl. Phys.* **B 665** (2003) 325, [hep-ph/0302135](#).
- [12] R. Harlander, *Higgs Production At The Large Hadron Collider: Theoretical Status*, *J. Phys. G* **35** (2008) 033001.
- [13] R.V. Harlander and K.J. Ozeren, *Finite top mass effects for hadronic Higgs production at next-to-next-to-leading order*, *JHEP* **0911** (2009) 088, [arXiv:0909.3420](#).
- [14] R.V. Harlander and K.J. Ozeren, *Top mass effects in Higgs production at next-to-next-to-leading order QCD: virtual corrections*, *Phys. Lett.* **B 679** (2009) 467, [arXiv:0907.2997](#).
- [15] A. Pak, M. Rogal, M. Steinhauser, *Finite top quark mass effects in NNLO Higgs boson production at LHC*, [arXiv:0911.4662](#).
- [16] A. Pak, M. Rogal, M. Steinhauser, *Virtual three-loop corrections to Higgs boson production in gluon fusion for finite top quark mass*, *Phys. Lett.* **B 679** (2009) 473, [arXiv:0907.2998](#).
- [17] S. Marzani, R.D. Ball, V. Del Duca, S. Forte, A. Vicini, *Higgs production via gluon-gluon fusion with finite top mass beyond next-to-leading order*, *Nucl. Phys.* **B 800** (2008) 127, [arXiv:0801.2544](#).
- [18] R. Harlander and P. Kant, *Higgs production and decay: Analytic results at next-to-leading order QCD*, *JHEP* **0512** (2005) 015, [hep-ph/0509189](#).
- [19] C. Anastasiou, S. Beerli, S. Bucherer, A. Daleo, Z. Kunszt, *Two-loop amplitudes and master integrals for the production of a Higgs boson via a massive quark and a scalar-quark loop*, *JHEP* **0701** (2007) 082, [hep-ph/0611236](#).
- [20] U. Aglietti, R. Bonciani, G. Degrassi, A. Vicini, *Analytic results for virtual QCD corrections to Higgs production and decay*, *JHEP* **0701** (2007) 021, [hep-ph/0611266](#).
- [21] S. Catani, M. Ciafaloni, F. Hautmann, *High-energy factorization and small x heavy flavor production*, *Nucl. Phys.* **B 366** (1991) 135.

- [22] R.D. Ball and R.K. Ellis, *Heavy quark production at high energy*, *Comp. Phys. Commun.* **0105** (2001) 053, [hep-ph/0101199](#).
- [23] G. Camici and M. Ciafaloni, *k-factorization and small-x anomalous dimensions*, *Nucl. Phys.* **B 496** (1997) 305; (E) *ibid.* **B 607** (2001) 431.
- [24] S. Catani and F. Hautmann, *High-energy factorization and small x deep inelastic scattering beyond leading order*, *Nucl. Phys.* **B 427** (1994) 475.
- [25] S. Marzani and R.D. Ball, *High Energy Resummation of Drell-Yan Processes*, *Nucl. Phys.* **B 814** (2009) 246, [arXiv:0812.3602](#).
- [26] G. Diana, *High-energy resummation in direct photon production*, *Nucl. Phys.* **B 824** (2010) 154, [arXiv:0906.4159](#).
- [27] F. Hautmann, *Heavy top limit and double-logarithmic contributions to Higgs production at $m_H^2/s \ll 1$* , *Phys. Lett.* **B 535** (2002) 159, [hep-ph/0203140](#).
- [28] S. Marzani, R. D. Ball, V. Del Duca, S. Forte, A. Vicini, *Finite-top-mass effects in NNLO Higgs production*, *Nucl. Phys. Proc. Suppl.* **186** (2009) 98, [arXiv:0809.4934](#).
- [29] R. Kirschner and M. Segond, *Small x resummation in collinear factorisation*, [arXiv:0910.5443](#).
- [30] R.K. Ellis and G. Zanderighi, *Scalar one-loop integrals for QCD*, *JHEP* **0802** (2008) 002, [arXiv:0712.1851](#).
- [31] The TEVNPH Working Group, *Combined CDF and D0 Upper Limits on Standard Model Higgs Boson Production with 2.1 - 5.4 fb^{-1} of Data*, FERMILAB-CONF-09-557-E, CDF Note 9998, D0 Note 5983.